Proceedings of the 2025 SICE Festival with Annual Conference
September 9-12, 2025, Chiang Mai, Thailand

A Hybrid SMC–FOC Strategy for BLDC Motor Control on a Low-Cost Real-Time Experimental Platform

Komarapat Nudad[1†], Peerayot Sanposh[2*], and Natthawut Chinthaned[3]

[1,2,3]Department of Electrical Engineering, Kasetsart University, Bangkok, Thailand
(Tel: +66-2-797-0999; E-mail: [1]komarapat.nu@ku.th, [2]peerayot.s@ku.ac.th, [3]fengnwc@ku.ac.th)
*Corresponding author: peerayot.s@ku.ac.th

Abstract: This paper proposes a hybrid control strategy that combines sliding mode control (SMC) and field-oriented control (FOC) for speed tracking of a brushless direct current (BLDC) motor. The outer loop, based on using SMC, enables fast response to load torque and external disturbances, while the inner loop, based on FOC with proportional–integral (PI) controllers, ensures precise control of torque and current. In the proposed hybrid SMC-FOC strategy, a fractional integral terminal sliding mode control (FITSMC) is selected, since it achieves faster and more accurate convergence while avoiding the need for unbounded control effort near the origin. Moreover, space vector pulse width modulation (SVPWM) is employed to further enhance system efficiency and reduce torque ripple. This hybrid SMC-FOC strategy was tested on a simple, low-cost ESP32 microcontroller. Experimental results demonstrate improved speed response and robustness compared to the conventional PI-FOC under both symmetric and asymmetric load conditions. These results suggested that the solution is practical for applications requiring affordable yet reliable motor control.

Keywords: fractional integral terminal sliding mode control (FITSMC), field oriented control (FOC), space vector pulse width modulation (SVPWM), torque ripple, ESP32

1. INTRODUCTION

1.1. Literature Reviw

Brushless direct current (BLDC) motors are widely used in various applications due to their high efficiency, compact design, silent operation, and reliability. These advantages make them well-suited for electric vehicles, robotics, and industrial automation applications [1]. The conventional Proportional–Integral (PI) controller has been widely applied, but often demonstrates limitations, including increased torque ripple and slower settling times under varying load conditions [2], [3].

Field-oriented control (FOC) is a widely used method that offers better torque and speed tracking control. In conventional FOC, referred to as PI-FOC, PI controllers are used in both inner and outer loops. However, it still faces difficulties when fast response and robust performance are simultaneously required, particularly in implementations on resource-constrained low-cost hardware platforms [4], [5].

Nonetheless, the PI-FOC continues to struggle with speed accuracy, sensitivity to disturbances, and parameter variations [6]. To overcome these issues, sliding-mode control (SMC) has been applied in the outer loop while PI controllers are still used in the inner loop. This SMC-FOC strategy offers superior disturbance rejection and dynamic performance. Experimental results demonstrate that the SMC–FOC approach yields better speed accuracy when compared to the PI-FOC [6].

Moreover, both PI-SMC and the incorporation of advanced modulation methods such as space vector pulse width modulation (SVPWM) can significantly enhance the efficiency of inverter voltage, minimize switching losses, and substantially reduce harmonic distortion compared to conventional PWM methods [7].

1.2. Motivation and Contributions

The motivation of this study is to enhance control performance by proposing a hybrid control strategy that combines SMC with FOC, and to validate its real-time feasibility using an ESP32 microcontroller. This approach aims to deliver improved dynamic performance, torque smoothness, and stability, with practical applicability in resource-constrained real-time systems.

The main contributions of this paper are as follows:

1. Hybrid SMC–FOC Control Design: A hybrid control strategy is proposed, FITSMC in the outer loop with FOC in the inner loop. The SMC-FOC combines fractional integral terminal sliding mode control (FITSMC) with the precision of FOC, enhanced through SVPWM

2. Low-Cost Real-Time Implementation: The proposed controller is implemented on an ESP32 microcontroller, demonstrating that advanced nonlinear control methods can be implemented on resource-constrained, low-cost embedded platforms without sacrificing performance.

3. Experimental Validation: The hybrid SMC-FOC is tested under both symmetric and asymmetric loads using a BLDC motor under symmetric and asymmetric loads.

4. Quantitative Performance Benchmarking: A comparative analysis against the PI–FOC controller is conducted using time-domain metrics and integral performance indices. The results demonstrate improvements in transient response, tracking accuracy, and reduction of speed ripple.

† Komarapat Nudad is the presenter of this paper.

1.3. Paper Organization

The remainder of this paper is organized as follows: Section 2 introduces preliminaries on the BLDC motor model and finite-time control. The proposed hybrid SMC–FOC strategy is presented in Section 3. In Section 4, the experimental setup is described. Results and discussion are given in Section 5. Section 6 concludes this paper.

2. PRELIMINARIES

2.1. BLDC Motor Model

2.1.1. BLDC Motor Model in abc reference frame

The electrical dynamic equations of Y-connected stator windings of a three-phase BLDC motor can be expressed in abc reference frame as follows [8]:

$$v_a = R_s i_a + L\frac{di_a}{dt} + e_a \tag{1}$$

$$v_b = R_s i_b + L\frac{di_b}{dt} + e_b \tag{2}$$

$$v_c = R_s i_c + L\frac{di_c}{dt} + e_c \tag{3}$$

where v_a, v_b, v_c are the phase voltages, i_a, i_b, i_c are the phase currents, and e_a, e_b, e_c are the induced back electromotive forces (EMFs). Here, R_s denotes the stator resistance, and the inductance L is defined as: $L = L_s - M$, where L_s is the stator inductance and M is the mutual inductance.

These electrical equations are based on the following assumptions: There is no change in the rotor reluctance with angle; the stator resistances of all phases are equal; the stator inductances of all phases are equal; the mutual inductance between phases is equal; and the stator currents are symmetric.

The relationship among the electrical rotor angle, electrical rotor speed, and mechanical rotor speed is given by the following.

$$\frac{d\theta_e}{dt} = \omega_e = \frac{P}{2}\omega_m \tag{4}$$

where ω_e is the electrical rotor speed and P is the number of poles.

The motor torque resulting from the electromagnetic force is given by [8]:

$$T_m = \frac{1}{\omega_m}(e_a i_a + e_b i_b + e_c i_c) \tag{5}$$

On the mechanical side, the motor dynamics is governed by:

$$J_m\frac{d\omega_m}{dt} + B_m\omega_m = T_m - T_L \tag{6}$$

where J_m is the inertia, B_m is the friction coefficient, and T_L is the load torque.

Assumption 1: The load torque $T_L(t)$ is bounded by a positive number Δ_{max}, i.e. $|T_L(t)| \leq \Delta_{max}$. ■

2.1.2. BLDC Motor Model in dq reference frame

To enable independent control of magnetic flux and motor torque [9], the BLDC motor equations are transformed from abc reference frame into dq reference frame. This transformation is accomplished using Park Transformation.

In dq reference frame, the electrical dynamic equations are given by:

$$v_d = R_s i_d + L\frac{di_d}{dt} - \omega_e L i_q \tag{7}$$

$$v_q = R_s i_q + L\frac{di_q}{dt} + \omega_e L i_d + e_q \tag{8}$$

where v_d and v_q are stator input voltage, i_d and i_q are stator current, $e_q = K_b\omega_m$ is the back EMF in dq reference frame.

Thus, the BLDC motor model is described by:

$$\frac{di_d}{dt} = -\frac{R_s}{L}i_d + \frac{P}{2}\omega_m i_q + \frac{1}{L}v_d \tag{9}$$

$$\frac{di_q}{dt} = -\frac{R_s}{L}i_q - \frac{P}{2}\omega_m i_d - \frac{K_b}{L}\omega_m + \frac{1}{L}v_q \tag{10}$$

$$\frac{d\omega_m}{dt} = -\frac{B_m}{J_m}\omega_m + \frac{1}{J_m}T_m - \frac{1}{J_m}T_L \tag{11}$$

Notably, the electromagnetic torque from Eq. (5) can be expressed in dq reference frame as:

$$T_m = K_t i_q \tag{12}$$

where K_t is the motor torque constant.

2.2. Finite-Time Control

Consider the nonlinear system given by:

$$\dot{s}(t) = f(t, s(t)),\ s(0) = s_0 \tag{13}$$

where $s \in \mathbb{R}^n$ is the system state, and $f : \mathbb{R}^+ \times \mathcal{D} \to \mathbb{R}^n$ is locally Lipschitz continuous with $f(t, 0) = 0, t > 0$.

Lemma 1: [10] Assume that there exists a continuously differentiable, positive definite function $V(s)$ on an open neighborhood $\mathcal{U}_0$ of the origin such that:

$$\dot{V}(s) \leq -\gamma V^{\alpha}(s),\ \forall s \in \mathcal{U}_0 \tag{14}$$

where $\gamma > 0$ and $0 < \alpha < 1$. Then, the origin is finite-time stable, and the reaching time is finite and satisfies the following inequality:

$$t_r(s_0) \leq \frac{1}{\gamma(1-\alpha)}V^{1-\alpha}(s_0) \quad ■ \tag{15}$$

3. HYBRID SMC-FOC STRATEGY

In this work, the hybrid SMC-FOC strategy is proposed for motor speed control. As shown in Figure 1, our control structure consists of four crucial components: an outer loop control, an inner loop control, the Park/Clarke Transformation, and the SVPWM module. The outer loop control utilizes FITSMC for robust speed regulation, while the inner loop control uses FOC for precise current and torque control.

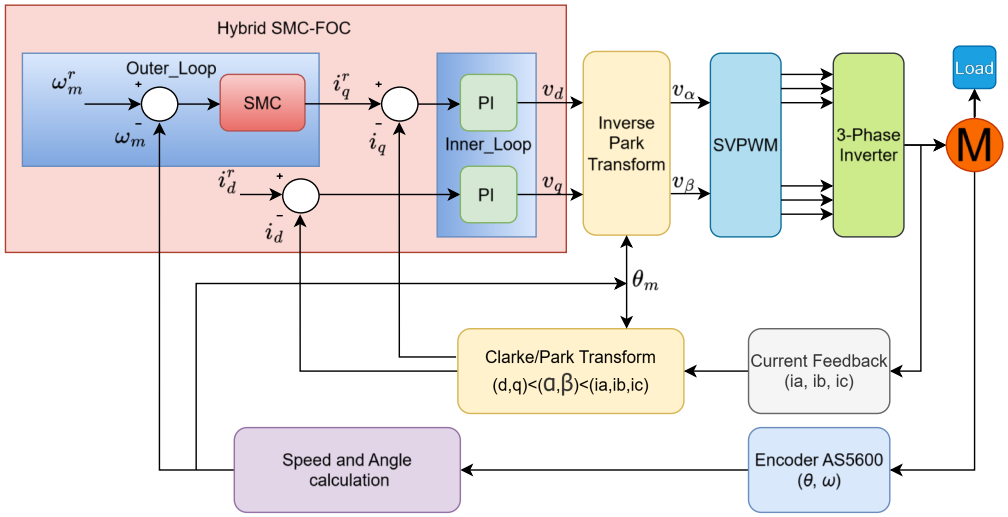

Fig. 1: Hybrid SMC-FOC strategy.

3.1. Outer Loop Control: SMC

In the outer loop, FITSMC is used to ensure that the rotor speed $\omega_m(t)$ follows the reference rotor speed $\omega_m^r(t)$ despite the existence of the unknown load torque T_L.

Since the cross-coupling terms $\frac{P}{2}\omega_m i_q$ and $\frac{P}{2}\omega_m i_d$ in Eq. (9) and (10) are eliminated by the inner-loop control design, as described in the next section, and given that the electrical time constant L/R_s is much smaller than the mechanical time constant J_m/B_m, the current dynamics are significantly faster than the mechanical dynamics. Therefore, only Eq. (11) is used to describe the motor speed dynamics.

Define the speed tracking error as:

$$e_\omega(t) = \omega_m^r(t) - \omega_m(t), \tag{16}$$

The FITSMC is defined by a sliding variable as follows [11]:

$$s(t) = e_\omega(t) + c\int_0^t e_\omega^{q/p}(\tau)\,\mathrm{d}\tau \tag{17}$$

where $c > 0$ is the integral gain, and p, q are positive odd integers satisfying $p > q > 0$.

Remark 1: [10] If the system is on the sliding surface: $s(t) = 0, \forall t \geq t_0$ with initial tracking error $e_\omega(t_0) = e_{\omega 0}$, the tracking error $e_\omega(t)$ converge to zero in finite settling time t_s given by:

$$t_s(e_{\omega 0}) = \frac{|e_{\omega 0}|^{1-q/p}}{c(1-q/p)} \quad \blacksquare \tag{18}$$

To find T_m, the following reaching law is chosen:

$$\dot{s} = -\varepsilon\, sgn(s) \tag{19}$$

where $\varepsilon > 0$ determines how fast it reaches the sliding surface.

By differentiating Eq. (17), we have:

$$\begin{aligned}\dot{s} &= \dot{e}_\omega + c\, e_\omega^{q/p} \\ &= [\dot{\omega}_m^r - \dot{\omega}_m] + c\, e_\omega^{q/p}\end{aligned} \tag{20}$$

By substituting $\dot{s}$ from Eq. (19) and $\dot{\omega}_m$ from Eq. (11) into Eq. (20), we obtain:

$$\begin{aligned}-\varepsilon\,\mathrm{sgn}(s) = \left[\dot{\omega}_m^r - \left(-\frac{B_m}{J_m}\omega_m + \frac{1}{J_m}T_m - \frac{1}{J_m}T_L\right)\right] \\ + c\, e_\omega^{q/p}\end{aligned} \tag{21}$$

Solving for T_m, we obtain:

$$\begin{aligned}T_m = J_m\left[\dot{\omega}_m^r + c\, e_\omega^{q/p} + \varepsilon\ \mathrm{sgn}(s)\right] \\ + B_m\omega_m + T_L\end{aligned} \tag{22}$$

Since all quantities on the right-hand side of Eq. (22) are known except T_L, the control law in Eq. (22) cannot be implemented.

By using the bound of T_L, the FITSMC is designed as follows:

$$\begin{aligned}T_m = J_m\left[\dot{\omega}_m^r + c\, e_\omega^{q/p} + \varepsilon\ \mathrm{sgn}(s)\right] \\ + B_m\omega_m + \Delta_{max}\,\mathrm{sgn}(s)\end{aligned} \tag{23}$$

Let $k = \varepsilon + \Delta_{max}/J_m$ be the FITSMC gain. Consequently, the FITSM is given by:

$$T_m = J_m\left[\dot{\omega}_m^r + c\, e_\omega^{q/p} + k\ \mathrm{sgn}(s)\right] + B_m\omega_m \tag{24}$$

Theorem 1: Under the assumptions of bounded torque load, the FITSMC given in Eq. (24) ensures that the tracking error converges to zero in a finite time, provided that $k > \Delta_{max}/J_m$. ■

To prove Theorem 1, consider the following candidate Lyapunov function [11]:

$$V_s = \frac{1}{2}s^2. \tag{25}$$

The derivative of $V(s)$ is given by

$$\begin{aligned}\dot{V}_s &= s\dot{s} \\ &= s\Bigg(\left[\dot{\omega}_m^r - \left(-\frac{B_m}{J_m}\omega_m + \frac{1}{J_m}T_m - \frac{1}{J_m}T_L\right)\right] \\ &\qquad + c e_\omega^{q/p}\Bigg) \end{aligned} \tag{26}$$

By substituting T_m from Eq. (24) into Eq. (26), we have:

$$\dot{V}_s = s\left(-k\,\mathrm{sgn}(s) - \frac{1}{J_m}T_L\right) = -k|s| - \frac{T_L}{J_m}s \tag{27}$$

From Assumption 1, $-\frac{T_L}{J_m}s \le |\frac{T_L}{J_m}s| \le \frac{\Delta_{max}}{J_m}|s|$. Consequently,

$$\dot{V}_s \le -\left(k - \frac{\Delta_{max}}{J_m}\right)|s| = -\gamma V_s^{1/2} \tag{28}$$

where $\gamma = \sqrt{2}\left(k - \frac{\Delta_{max}}{J_m}\right)$.

According to Lemma 1, $\gamma > 0$, or equivalently, the controller gain k must satisfy $k > \Delta_{max}/J_m$ to guarantee finite reaching time t_r, which is given by Eq. (15).

Moreover, the settling time t_s, given by Eq. (18), is also finite. Consequently, the convergence time—equals the sum of t_r and t_s—is also finite. ■

3.2. Inner Loop Control: FOC

In the inner loop, FOC with two PI controllers and a decoupling method is used for controlling the direct-axis current i_d and quadrature-axis current i_q, such that they track the reference currents i_d^r and i_q^r, respectively, given by:

$$i_d^r = 0 \tag{29}$$

$$\begin{aligned} i_q^r &= \frac{T_m}{K_t} \\ &= \frac{J_m}{K_t}\left[\dot{\omega}_m^r + c\, e_\omega^{q/p} + k\ \mathrm{sgn}(s)\right] + \frac{B_m}{K_t}\omega_m \end{aligned} \tag{30}$$

Define the speed tracking error as:

$$e_d = i_d^r(t) - i_d(t) \tag{31}$$

$$e_q = i_q^r(t) - i_q(t) \tag{32}$$

The PI controllers, combined with the decoupling method, can be designed as:

$$v_d = v_d^{'} - L\frac{P}{2}\omega_m i_q \tag{33}$$

$$v_q = v_q^{'} + L\frac{P}{2}\omega_m i_d + K_b\omega_m \tag{34}$$

where $v_d^{'}$ and $v_q^{'}$ are the outputs of the PI controllers:

$$v_d^{'} = K_p e_d + K_i\int_0^t e_d(\tau)d\tau \tag{35}$$

$$v_q^{'} = K_p e_q + K_i\int_0^t e_q(\tau)d\tau \tag{36}$$

where $K_p > 0$ and $K_i > 0$ denote the proportional and integral gains. For simplicity, the same gains are applied to both i_d and i_q control loops.

Thus, the current dynamics are now described by:

$$\frac{di_d}{dt} = -\frac{R_s}{L}i_d + \frac{1}{L}v_d^{'} \tag{37}$$

$$\frac{di_q}{dt} = -\frac{R_s}{L}i_q + \frac{1}{L}v_q^{'} \tag{38}$$

Figure 2 illustrates the block diagram of the PI control loop for i_q. The structure for i_d is similar. For brevity, only the PI controller design for the i_q loop is shown.

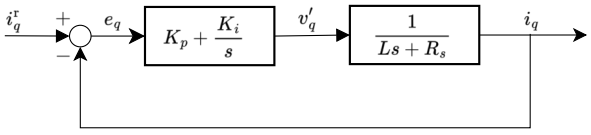

Fig. 2: Block diagram of PI current control loops

To design the PI controller for the i_q loop, consider the following open-loop transfer function:

$$G_{OL}(s) = \frac{K_p + K_i/s}{Ls + R_s} = \frac{K_p}{Ls}\left(\frac{s + K_i/K_p}{s + R_s/L}\right) \tag{39}$$

By choosing $K_i/K_p = R_s/L$, we have:

$$G_{OL}(s) = \frac{K_p}{Ls} \tag{40}$$

Thus, the closed-loop transfer function for i_q is given by:

$$\frac{I_q(s)}{I_q^r(s)} = \frac{G_{OL}(s)}{1 + G_{OL}(s)} = \frac{K_p}{Ls + K_p} \tag{41}$$

By choosing a large K_p/L, we obtain:

$$\frac{I_q(s)}{I_q^r(s)} = \frac{K_p/L}{s + K_p/L} \approx 1 \tag{42}$$

and the transient response time of i_q is very short.

Consequently, both current loops can be made sufficiently fast by proper tuning of the PI controller gains. Therefore, the current dynamics in the inner loop are significantly faster than the mechanical dynamics in the outer loop.

4. EXPERIMENTAL SETUP

As shown in Figs. 3 – 5, all experiments were conducted on a Gimbal BLDC2804 motor equipped with Hall sensors and driven by an SVPWM-based three-phase inverter, under the control of an ESP32 microcontroller. Speed and position feedback were obtained from an AS5600 encoder, while phase currents were measured using an ACS712 current transducer. Motor speed, torque estimates, and phase currents were logged to a host PC for post-processing in MATLAB, enabling quantitative comparison between the hybrid SMC–FOC and conventional PI-FOC under both symmetric and asymmetric loading conditions.

Notably, in all experiments, the signum function in the hybrid SMC-FOC is replaced with a smooth approximation using the hyperbolic tangent function, defined as $\tanh(s/\epsilon)$, $\epsilon = 0.6$, to mitigate chattering effects.

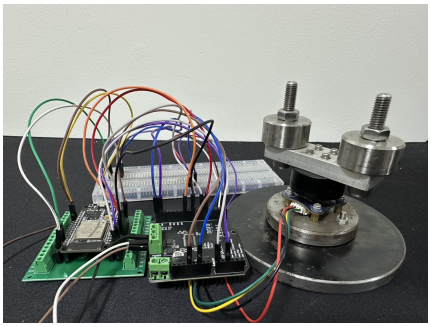

Fig. 3: Experimental setup

(a) Symmetric load (b) Asymmetric load

Fig. 4: Motor and encoder under symmetric and asymmetric loading conditions

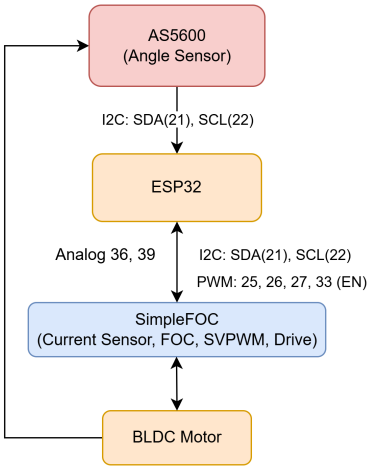

Fig. 5: System overview on ESP32-based motor control

5. RESULTS AND DISCUSSION

The proposed hybrid SMC–FOC controller was tested on an ESP32 platform under two loading conditions: (1) symmetric load at 1,000 RPM and (2) asymmetric load at 200 RPM. Although the experiment was conducted for 10 seconds, only the first 3 seconds are presented in Figs. 6 and 7 for clarity. The speed and torque measurements were acquired in real-time and plotted at a sampling interval of 0.1 seconds.

The following time-domain metrics and integral performance indices were used:

1. Percent overshoot
2. Rise time (10% – 90% criteria)
3. Settling time (2% criteria)
4. Steady-state error
5. Integral square error (ISE)
6. Integral absolute error (IAE)
7. Integral time absolute error (ITAE)

5.1. Motor Responses under Symmetrical Load

The motor responses under the symmetric load are shown in Fig. 6. The proposed SMC–FOC controller achieved faster and smoother speed response with lower speed ripple compared to the conventional PI–FOC.

Furthermore, the torque response of the SMC–FOC exhibited a less steep transient and lower steady-state torque than that of the PI-FOC, indicating improved power efficiency.

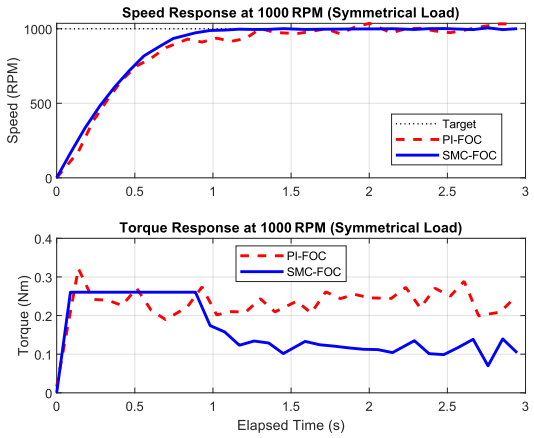

Fig. 6: Responses under symmetric load.

As summarized in Table 1, all time-domain metrics and integral performance indices for the proposed SMC-FOC showed notable improvements over those of the PI–FOC.

Table 1: Performance metrics under symmetric load

Metrics	PI-FOC	SMC-FOC
Overshoot (%)	5.13	0.97
Rise Time (s)	0.6349	0.6328
Settling Time (s)	1.2202	0.9301
Steady-State Error (RPM)	–5.03	–0.99
ISE	238,248.13	198,528.88
IAE	543.63	362.66
ITAE	982.85	243.41

5.2. Motor Responses under Asymmetrical Load

The motor responses under asymmetric loading conditions at 200 RPM are illustrated in Fig. 7. The hybrid SMC–FOC had more accurate speed tracking with a very small overshoot and shorter settling time. Specifically, the speed response exhibited a sharp rise to the target speed with a small steady-state error. Whereas, the PI–FOC exhibited a significant overshoot and prolonged oscillations.

Moreover, the SMC–FOC produced a lower initial torque spike and reduced steady-state torque ripple compared to the PI–FOC, indicating improved control smoothness and reduced mechanical stress.

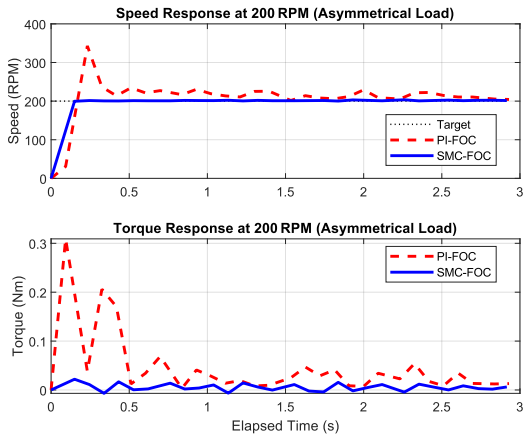

Fig. 7: Responses under asymmetric load.

As shown in Table 2, the SMC–FOC reduced overshoot from 69.38% to 2.32%, and settling time from 9.16 s to 0.15 s, while also improving all integral performance indices. These results highlighted the improvements in dynamic response, tracking accuracy, and speed ripple reduction of the SMC–FOC strategy under asymmetric load.

Table 2: Performance metric under asymmetric load

Metric	PI-FOC	SMC-FOC
Overshoot (%)	69.38	2.32
Rise Time (s)	0.0498	0.1000
Settling Time (s)	9.1621	0.1500
Steady-State Error (RPM)	2.60	–1.17
ISE	8,001.72	1,460.65
IAE	122.58	24.98
ITAE	331.58	68.49

6. CONCLUSION AND FUTURE WORK

The proposed hybrid SMC–FOC strategy with SVPWM, implemented on the ESP32 platform, delivered noticeably lower speed ripple, higher speed accuracy, and more robustness than the baseline PI-FOC under both symmetric and asymmetric load conditions. Future work will focus on adaptive control, on-the-fly gain tuning, and validation over a broader range of operating speeds and loads.

ACKNOWLEDGMENT

The authors gratefully acknowledge the support and resources provided by the Department of Electrical Engineering, Faculty of Engineering, Kasetsart University. This work was conducted as part of the Master's Degree Program in Electrical Engineering at Kasetsart University.

REFERENCES

[1] V. Kumar, K. Chenchireddy, K. R. Sreejyothi, and G. Sujatha, "Design and development of brushless dc motor drive for electrical vehicle application," in *AI Enabled IoT for Electrification and Connected Transportation*. Springer, 2022, pp. 201–217.

[2] A. M. Ahmed, A. Ali-Eldin, M. S. Elksasy, and F. F. Areed, "Brushless dc motor speed control using both pi controller and fuzzy pi controller," *International Journal of Computer Applications*, vol. 109, no. 10, pp. 29–35, 2015.

[3] M. Mahmud, M. R. Islam, S. Motakabber, M. D. A. Satter, K. E. Afroz, and A. A. Habib, "Control speed of bldc motor using pid," in *2022 IEEE 18th International Colloquium on Signal Processing & Applications (CSPA)*. IEEE, 2022, pp. 150–154.

[4] L. Baghli, E. Jamshidpour, and N. Takorabet, "Linear bldc motor embeded control on esp32," in *2024 3rd International Conference on Advanced Electrical Engineering (ICAEE)*, 2024, pp. 1–6.

[5] A. Bosso, C. Conficoni, D. Raggini, and A. Tilli, "A computational-effective field-oriented control strategy for accurate and efficient electric propulsion of unmanned aerial vehicles," *IEEE/ASME Transactions on Mechatronics*, vol. 26, no. 3, pp. 1501–1511, 2021.

[6] P. Shah, P. Ubare, D. Ingole, and D. Sonawane, "Performance improvement of bldc motor speed control using sliding mode control and observer," in *2021 International Symposium of Asian Control Association on Intelligent Robotics and Industrial Automation (IRIA)*. IEEE, 2021, pp. 247–252.

[7] V. K. U and P. S., "Analysis of bldc motor performance using space vector pulse width modulation," in *2016 International Conference on Computation of Power, Energy Information and Commuincation (ICCPEIC)*, 2016, pp. 549–552.

[8] R. Krishnan, *Permanent Magnet Synchronous and Brushless DC Motor Drives*, 1st ed. Boca Raton: CRC Press, 2010, eBook published on December 19, 2017.

[9] M. N. Gujjar and P. Kumar, "Comparative analysis of field oriented control of bldc motor using spwm and svpwm techniques," in *2017 2nd IEEE International Conference on Recent Trends in Electronics, Information & Communication Technology (RTEICT)*, 2017, pp. 924–929.

[10] Y. Liu, H. Li, Z. Zuo, X. Li, and R. Lu, "An overview of finite/fixed-time control and its application in engineering systems," *IEEE/CAA Journal of Automatica Sinica*, vol. 9, no. 12, pp. 2106–2120, Dec. 2022.

[11] C.-S. Chiu, "Derivative and integral terminal sliding mode control for a class of mimo nonlinear systems," *Automatica*, vol. 48, no. 2, pp. 316–326, 2012.